Explicit Modelling of Spectral Bandshapes by a Mixed Quantum-Classical Approach: Solvent Order and Temperature Effects in the Optical Spectra of Distryrylbenzene

Javier Cerezo, Johannes Gierschner, Fabrizio Santoro and Giacomo Prampolini

Explicit Modelling of Spectral Bandshapes by a Mixed Quantum-Classical Approach: Solvent Order and Temperature Effects in the Optical Spectra of Distryrylbenzene

Javier Cerezo,[a,b] Johannes Gierschner,[c]
Fabrizio Santoro[b,*] and Giacomo Prampolini[b,*]

[a]*Departamento de Química and Institute for Advanced Research in Chemical Sciences (IAdChem),*
Universidad Autónoma de Madrid
28049 Madrid, Spain
[b]*Istituto di Chimica dei Composti OrganoMetallici* (ICCOM),
Consiglio Nazionale delle Ricerche (CNR),
Area della Ricerca, via G. Moruzzi 1, I-56124 Pisa, Italy
[c]*Madrid Institute for Advanced Studies, IMDEA Nanoscience*
C/ Faraday 9, Ciudad Universitaria de Cantoblanco, 28049, Madrid, Spain

[*]fabrizio.santoro@pi.iccom.cnr.it, giacomo.prampolini@pi.iccom.cnr.it

Abstract

The absorption and emission spectral shapes of a flexible organic probe, the distyrylbenzene (DSB) dye, are simulated accounting for the effect of different environments of increasing complexity, ranging from a homogeneous, low-molecular-weight solvent, to a long-chain alkane, and, eventually, a channel-forming organic matrix. Each embedding is treated explicitly, adopting a mixed quantum-classical approach, the Adiabatic Molecular Dynamics – generalized vertical Hessian (Ad-MD|gVH) model, which allows a direct simulation of the environment-induced constraining effects on the vibronic spectral shapes. In such a theoretical framework, the stiff modes of the dye are described at a quantum level within the harmonic approximation, including Duschinsky mixing effects, while flexible degrees of freedom of the solute (e.g. torsions) and those of the solvent are treated classically by means of molecular dynamics sampling. Such a setup is shown to reproduce the distinct effects exerted by the different environments in varied thermodynamic conditions. Besides allowing for a first-principles rationale on the supramolecular mechanism leading to the experimental spectral features, this result represents the first successful application of the Ad-MD|gVH method to complex embeddings and supports its potential application to other heterogeneous environments, such as for instance pigment-protein complexes or organic dyes adsorbed into metal-organic frameworks.

1 Introduction

Conjugated organic materials have found immense interest as active compounds in materials and life science applications. [1] This is especially due to the large variability of the organic route to generate tailor-made chromophores with fine-tuned absorption and emission colors and intensities. [2] In recent years, there is particular interest in 'color pureness', which is decided by the width of the emission band, [3, 4] whose shape is in turn determined by two factors. On the one hand, the homogeneous spectral broadening is mainly connected to the chromophore, i.e. to its geometrical change upon electronic excitation (which can largely vary, depending on the specific molecular structure), [5] and by the coupling efficiency of the various intramolecular vibrational modes. On the other hand, the total width is also largely influenced by the inhomogeneous broadening, stemming from environmental effects as the thermodynamic conditions or the nature and ordering of the embedding. In the quest of a rational molecular design through computational approaches, a reliable modelling of spectral shapes through both intramolecular and environmental contributions is therefore decisive. Environmental spectral broadening results from the subtle interplay between the nuclear motion of the photoactive molecule and the fluctuations of the embedding medium. In fact, the sensitivity of the dye's structure to the constraints exerted by the environment eventually reflects into the response to the electronic transition, and crucial information about the interaction between the probe and its chemical background is hence encoded in the resulting electronic spectrum. [3, 4, 6] This scenario is even more evident when the dye contains some flexible coordinates, which are expected to be more influenced by the supramolecular embedding.

From a computational point of view, methods to simulate the spectral shape can nowadays deliver vibronic spectra readily comparable to experiments for semirigid molecules, i.e. whose potential energy surfaces (PESs) can be properly described with the harmonic approximation, within simple solvents, usually described with polarizable continuum models. [7–11] In fact, a number of effective time-independent (TI) [12–16] and time-dependent (TD) [17–20] approaches, based respectively on sum-over-states or Fourier transform of correlation functions, are nowadays available to account in an automatic way for the vibronic shape due to

the intramolecular modes of medium to large dyes (hundreds of vibrations), at any temperature. Nonadiabatic effects can also be described with effective quantum dynamical simulations, [21, 22] driven by linear or quadratic vibronic Hamiltonians. [23–25] Yet, the inclusion of flexible degrees of freedom challenges this kind of calculation, by preventing the adoption of harmonic models to describe the potential along the coordinates expected to undergo rather large deformations during their dynamics. Moreover, the effect of complex environments, thus able to establish local and specific interactions with the molecular probe, requires the use of explicit models to account for its heterogeneity. Both issues can be solved by adopting a hybrid quantum-classical scheme, where the flexible coordinates and solvent fluctuations are treated classically, while stiff modes retain a quantum description. Solute flexibility and environment fluctuations can be described with classical Molecular Dynamics (MD). In order to re-introduce quantum vibronic effects along a MD trajectory different approaches have been proposed, [26–30]. A powerful approach which adopts cumulant expansions [31] and uses response functions obtained by sampling excitation energy fluctuations with classical MD, is gaining increasing popularity especially in applications in complex bio-systems [32–34]. It is usually limited to describe linear couplings through spectral densities, but recent developments promise to be able to handle also in an accurate way quadratic couplings effects (Duschinsky mixings). [35] In this context, some of us recently followed a different route, introducing the Ad-MD|gVH method, [36] a mixed quantum classical approach rooted in such stiff/flexible mode partitions. In its first implementations, Ad-MD|gVH was shown to accurately reproduce absorption and emission spectra of organic dyes of increasing flexibility embedded in different solvents, able to settle specific interactions as hydrogen bonds. [36–38]

In order to systematically tackle environmental effects at a computational level, a suitable test system with extensive experimental data is required, where one would ideally vary systematically only one parameter of the mentioned variable space (e.g. temperature or the embedding environment), while keeping the others constant. An ideal test system in this respect is distyrylbenzene (DSB), [39] being a textbook example for a highly emissive chromophore with an essentially planar equilibrium structure, but at the same time, high (torsional) flexibility, see Figure 1.a. Furthermore, DSB possesses a simple structure of a 'naked' conjugated hydrocar-

bon, and is thus not expected to induce strong interactions with the surrounding environment, which simplifies the theoretical description of solute-embedding interactions. Importantly, DSB was investigated experimentally in a multitude of different environments, e.g. (i) in various fluid solvents at room temperature,[24,25] (ii) in solid solution (e.g. poly-methylmethacrylate), [40] (iii) in stretched polyethylene sheets, [41] (iv) adsorbed on alumina or silica surfaces, [42] (v) embedded in channel-forming solid organic matrices. [43–47](vi) at low temperature conditions in glassy solvents [46] and Shpolskii matrices (e.g. tetradecane), [46, 48] as well as (vii) in (nano)crystalline phases. [39, 49–51] Previous computational approaches towards the spec-

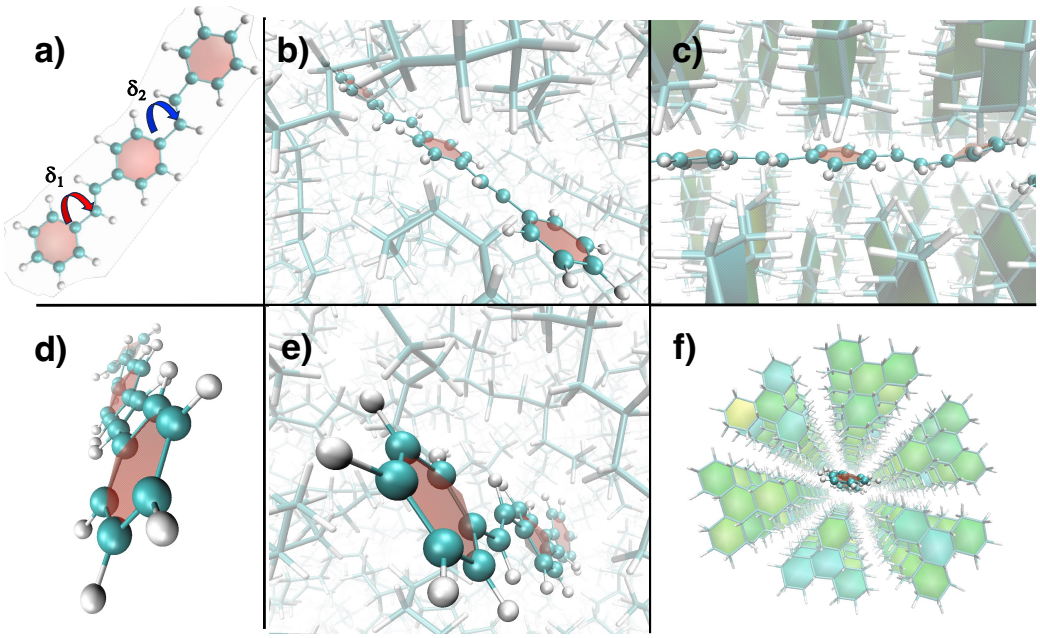

Figure 1: Side (top panels) and top (bottom panels) views of the different systems modelled in the present study. a,d) DSB isolated chromophore, including the labels of flexible torsions, δ_1 and δ_2; b,e) DSB in *n*-tetradecane, side view; c,f) DSB in PHTP matrix.

tral bandshape of DSB in solution focused on atomistic calculations of vibronic coupling of single molecules without explicit inclusion of the solvent, [46] but accounting for the thermal population of low-frequency torsional modes in the ground and first excited state (S_0, S_1) in a full quantum-chemical [46] and semi-classical manner, relying on the harmonic approximation. [46, 47] Within this approach, and using an empirical Gaussian broadening to account for the solvent effects, excellent agreement for the room temperature band shapes was obtained,

correctly reproducing the experimentally observed breakdown of the mirror symmetry between absorption and emission spectra. [46] It should be further mentioned in this context that intermolecular aggregation effects on spectral bandshapes were intensively tackled through (empirically parametrized) combined excitonic coupling and linear exciton-phonon coupling for absorption and emission spectra of DSB, [52] as well by atomistic QM/MM calculations of DSB crystal emission. [50] In the context of the current work, previous experimental and theoretical work reported the peculiar behaviour registered in DSB electronic response to either temperature alteration or variation of the embedding. [46,47] It was therefore hypothesized that such features could be traced back to the different flexibility, in the ground with respect to the excited electronic state, of the torsions around single bonds (see Figure 1.a). Such flexibility is expected to be largely affected by the characteristics of the environment in which the DSB molecule is dispersed. In particular, it has been demonstrated experimentally that the introduction of DSB into a perhydrotriphenylene (PHTP) matrix (see Figures 1.c and 1.e) has a significant impact on the spectral shape of absorption, resulting in narrow bands with well-defined vibrational features [46, 47]. More specifically, the absorption spectrum undergoes significant changes in going from EPA, a glass-forming solvent mixture of diethyl ether, methylbutane and ethanol, to a nano-structured environment as the PHTP matrix. The interplay between torsions and the constraints imposed by the embedding are therefore key to tune the spectral shape. The simultaneous necessity to account for vibronic structure and for intrinsic flexibility of the molecule with the possible steric limitations due to the environment makes therefore this system an ideal playground to investigate the performance of Ad-MD|gVH method. Moreover, experimental spectra for DSB are available in different environments and conditions, including very low temperatures (a few Kelvin). In such extreme conditions (and within embeddings where the mobility of the particles is practically restricted, as in crystals), sampling with MD simulations may be thought to be not relevant, as the low temperature may challenge the classical approximation. Nevertheless, also in this case, the description of the environment through QM/MM calculations might reveal essential. For instance, Shuai and co-workers described the effect of very high pressures on the photophysics of mechano-responsive luminescent crystals by carrying out QM/MM calculations to evaluate the Hessian of one dye, treated at QM level,

while the relative position of each dye in the crystal is consistent with the targeted pressure [53]. Similarly, the mechanical response of individual poly-pyrenylene chains upon detachment from a gold surface, as determined with an atomic force microscopic at 5 K, was successfully reproduced [54, 55] by classical Molecular Dynamics (MD) simulations, carried out with Quantum Mechanical Derived Force-Fields (QMD-FFs). [56–59] Finally, as far as DSB is specifcally concerned, QM/MM calculations were pivotal for a successful reproduction of the low temperature emission signal. [50] Therefore, we will apply the Ad-MD|gVH MD/QM sequential protocol to DSB at room and low (10K) temperature within two distinct embeddings, namely tetradecane and a PHTP matrix (see Figure 1). In this framework, we will show that Ad-MD|gVH provides an easy to implement approach to include out-of-equilibrium effects accounting for the constraints of the environments.

2 Method

The Ad-MD|gVH approach [36] is based on a partition in "stiff" and "soft" degrees of freedom (DoFs), characterized respectively by small amplitude oscillations or an enhanced flexibility allowing for larger distortions. Stiff modes of the target dye are described with harmonic potentials, treated quantum mechanically, while the soft modes related to its more flexible coordinates are accounted for at classical level, sampling the trajectories produced by statistically meaningful MD runs, carried out with accurate QMD-FFs. The DoFs of the surrounding environment can also be considered soft modes, and hence treated explicitly with a classical MD.

In short, this protocol implies running first a MD simulation, from which a number of snapshots (typically, around 100) are extracted. For each configuration, the Hessians for the initial and final states of the electronic transition are computed at QM/MM level, and all the soft modes are projected out from the coordinate space. The resulting reduced Hessians are subsequently used to compute the vibronic spectra, reconstructing the harmonic potentials for the initial and final states at each snapshot. This strategy is grounded on an adiabatic ansatz, in which the projected coordinates are the slow ones, and they are accounted for classically (i.e., from the MD sampling), whereas harmonic surfaces of the stiff (fast) coordinates are computed specifically for each configuration for the soft (slow) modes at each snapshot, thus introducing the

coupling between the two coordinates sets. The vibronic calculations on the reduced dimensionality spaces are performed within a TD framework, [10] which allows for fast computations and the effective inclusion of the temperature effects for stiff modes, consistently with the soft modes, thermally averaged by the sampling along the classical MD trajectories.

The whole process, summarized in Figure 2, relies on the accuracy of the MD trajectory; therefore, the force field (FF) adopted is an essential part of the calculation. For this reason, the first step involves the parametrization of a QMD-FF [56, 58] for each of the initial states of the electronic transition of interest (ground state, S_0, for absorption and lowest excited state, S_1, for emission). In fact, in order to obtain accurate spectra and make a proper sampling of the

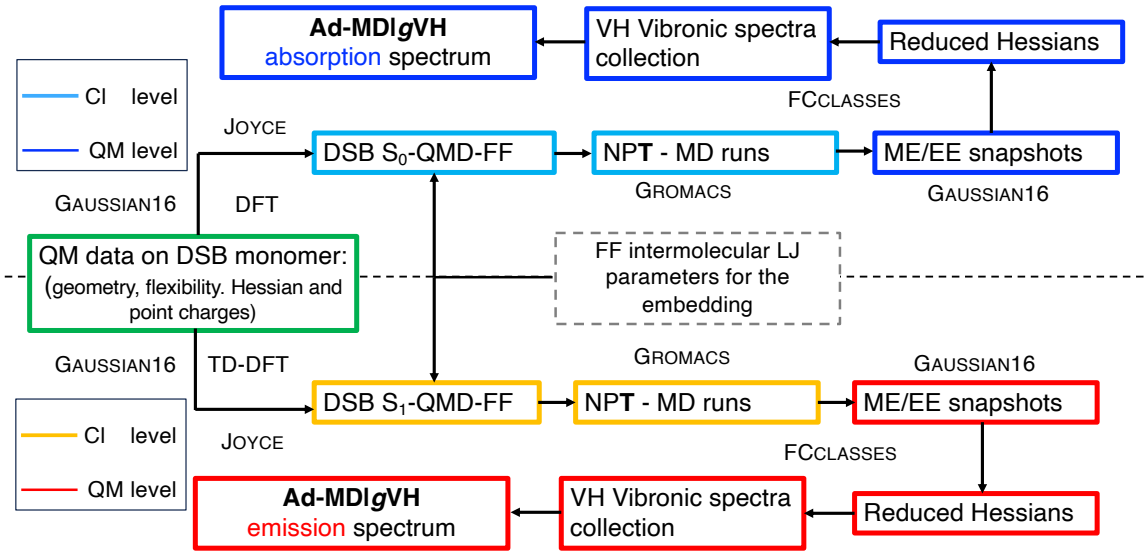

Figure 2: Summary of the Ad-MD|gVH protocol adopted in this work for the absorption (top, blueish colors) and emission (bottom, reddish colors) spectra of the DSB flexible dye at varied thermodynamic conditions (T) and in different embeddings. Steps carried out either at classical (Cl) or quantum-mechanical (QM) level are evidenced with cyan/orange or blue/red frames, from absorption or emission, respectively. Additionally, the software packages employed throughout the protocol are also reported along the scheme.

configurational space of the system, it is important that the adopted FFs are fully consistent with the underlying chosen electronic structure method. To describe the conformational dynamics of DSB, therefore, we adopt a QMD-FF intramolecular term parameterized with the JOYCE pro-

cedure, [56, 58, 60] which is designed to derive consistent ground and*, more noticeably,* excited FFs from reference QM training data. [36, 38, 61–64] It is worth noting that, for each considered electronic state, only one FF is parameterized for the DSB dye, and used in all environments (see Section A in the Supporting Information, SI, for further details). To that end, target QM data for the parameterization are computed in the gas phase. These were obtained based on either density functional theory (DFT) or on its TD extension (TD-DFT), for S_0 or S_1, respectively. Thus, the specificity of each environment on the DSB molecule is solely encoded in the intermolecular FF parameters, Coulomb and Lennard-Jones (LJ), ruling the non-bonded interactions between the dye and the surrounding system. The dependence of such intermolecular interactions on the electronic state of the DSB dye is also included in the model, as the QMD-FF point charges determining the Coulomb interaction are also derived from QM descriptors, namely from the DFT/TD-DFT electronic density through the RESP procedure while accounting for the average solvent effect at PCM level. [7] The resulting S_0 and S_1 QMD-FFs are employed in MD runs carried out on systems containing the dye and the considered embeddings and simulated in realistic conditions at controlled pressure and temperature.

The sampling is thereafter performed along the thermalized MD trajectory, which contains configurations where all DoFs of the chromophore are displaced with respect to its minimum energy structure. On each of these frames, a vibronic model is built from energies, gradients and Hessians computed through a QM/MM model (with DSB in the QM layer) by (i) projecting out the flexible degrees of freedom of DSB as well as those of the solvent, and (ii) locating the local harmonic approximation (LHA) minimum corresponding to the stiff DoFs retained in the model for both the initial and final electronic states (gVH model). The projection of flexible coordinates from the solute is carried out with an iterative scheme in internal curvilinear coordinates, updating both the projector and the metric of the space at each iteration. [36] The same partition in harmonic and flexible sets is applied to all snapshots in different environments. The final spectra, accounting for all DoFs, are obtained by averaging over all individual spectra computed at each snapshot with the reduced harmonic space. The whole procedure is summarized in Figure 2, while further details can be found in the original paper. [36]

3 Computational details

All QM calculations were performed using GAUSSIAN16 program [65], at DFT or TD-DFT level with CAM-B3LYP functional and the 6-31+G(d,p) basis set. Some test calculations were also carried out with PBE0, M06-2X, ωB97XD and M11 functionals, as well as with MP2, using the same 6-31+G(d,p) basis set in all cases. Additional calculations on the excited states were instead performed with ADC(2) using SV(P) and aug-cc-pVDZ basis set with Turbomole [66] and with 6-31+G(d,p) with Psi4 [67]. As sketched in Figure 2, the S_0 and S_1 QMD-FFs for DSB are fitted against QM data using the JOYCE code [68], exploiting Hessian and potential energy scan along flexible coordinates, computed at either DFT and TD-DFT level. The standard multistep JOYCE protocol was adopted, [36,38,56,58,69] first assigning the force constants of stiff coordinates and subsequently setting the coefficients of the Fourier-like terms that describe flexible coordinates. A detailed description of the parameterization procedure can be found in the Section A of the SI.

MD simulations were carried out with GROMACS [70], on three different systems, namely the isolated dye, one DSB molecule embedded in 930 *n*-tetradecane molecules or three DSB molecules dispersed in a pre-equilibrated nano-structured channel, composed by 72 PHTP units. All systems were first equilibrated, keeping the temperature and, for condensed phase simulations, also the pressure constant with the Berendsen thermostat and barostat algorithms [71] respectively. Successively, the production runs were performed with the Bussi-Parrinello thermostat [72] and (for condensed phase simulations) the Parrinello-Ramhan barostat [73], which, in principle, ensure a true isothermal-isobaric (or canonical, for gas phase simulations) ensemble. Non-bonded interactions were evaluated with a cut-off of 11Å for van der Waals and using PME [74] for electrostatics. A time-step of 1 fs was adopted, applying constraints to all bonds involving hydrogen atoms with the LINCS algorithm [75]. Production runs were conducted for a total time of 10 ns. In the case of the simulations at 10 K , the initial conformation is generated by gradually lowering the temperature, keeping the solute frozen at its equilibrium geometry until 50 K, thereafter releasing all constraints, allowing for thermal equilibration. We note that the simulation of the cooling state is far from trivial and our simple choice (named in

SI Route I) may result in a too limited conformational sampling. In the SI we show an additional cooling route (Figure S5), in which the solute may move while cooling, thus exploring a number of accessible conformations to ensure proper sampling of different conformations blocked in the frozen state. This second strategy (Route II) results into a significantly larger conformational distribution (see for instance Figure S6), which eventually leads to an excessive spectral broadening.

Along the MD trajectories, snapshots are extracted every 100 ps, generating a total of 100 snapshots for each scenario (i.e different embeddings, different temperature, different electronic state). Hessians at each snapshot were computed with an ONIOM scheme in which the dye (DSB) is included in the QM layer, and all solvent molecules with any atom within 4 Å of the dye are treated with the MM potential used in the MD simulation, while the remaining solvent atoms within a sphere of 35 Å are treated as point charges (using the partial charges adopted in the MD simulation). The inclusion of a first MM sphere improves the computation of gradients and Hessians as discussed in Ref. [36]. The reduced spaces on which vibronic lineshapes are computed are generated by the iterative projection [36] of the four torsions around single C-C bonds, after defining each of them as the linear combination with an equal weight of the four dihedrals involved. Additionally, the four pyramidalizations over carbon atoms involved in the double bonds along the chain, directly identified with the corresponding improper dihedrals, are also projected out. Both the iterative projections and the subsequent calculation of the vibronic lineshapes on the reduced spaces were carried out with $\mathscr{FC}classes3$ [69]. Vibronic spectra include a very small broadening (HWHM=0.01 eV), which is required to avoid numerical issues in the Fourier transform and provides a convenient way to partially correct the incompleteness of the sampling, by reducing the noise without affecting the width of the spectrum. Static vibronic spectra were also computed for pre-screening the performance of different DFT functional adopting Vertical Hessian (VH) and Adiabatic Hessian (AH) harmonic models, [76] and standardized TD protocols implemented in $\mathscr{FC}classes3$ [69].

In this study we mainly aim to investigate the intra- and inter-molecular factors that break the symmetry between the shape of DSB's absorption and emission spectra and how they are modulated in different environments. For this reason, we display spectra in the energy (and

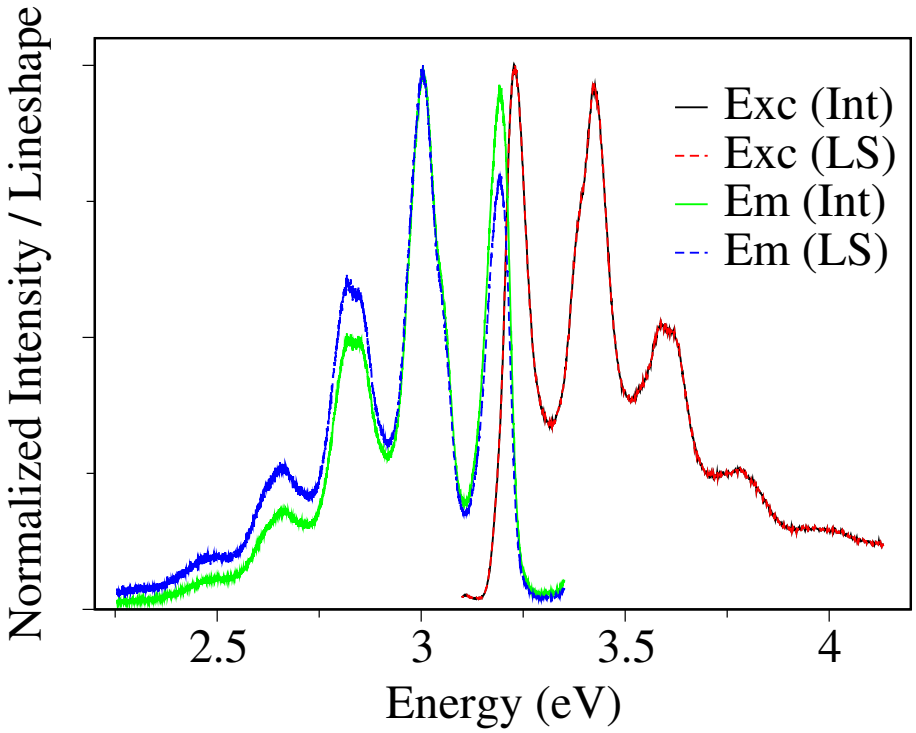

Figure 3: Relative lineshape and intensity emission and excitation spectra of DSB in EPA at 10 K, from the recorded experimental data in ref. [47]. Transformations from intensity (i.e., direct experimental signal) to lineshape are indicated in the text.

not in the wavelength) domain, as already done in the original papers were the experimental data were taken from [46, 47]. Moreover, in some cases we transform both experimental and computed emission spectra from intensities to lineshapes $L(\omega)$, as

$$L(\omega) = NI(\omega)/\omega^3$$

that is by dropping out the dependency on the photon energy. [77]

N is a normalization factor applied to the computed spectra e(xperimental spectra in refs. [46, 47] were already normalized or reported in arbitrary units). Since, instead of absorbance, for analysing absorption the original paper actually provides fluorescence excitation spectra, no ω-dependent correction has to be applied, because, in the limit of constant photon density, the fluorescence excitation signals and lineshapes are expected to be superimposed. The difference between intensity and lineshape spectra can be appreciated in Figure 3. The latter ones provide a better framework to analyze differences in the spectral shapes for emission and absorption,

as for instance lineshapes are expected to be exactly mirror-symmetric [78, 79] in the Condon approximation (bright transitions) and when the initial and final state PES are harmonic and have no difference apart from a shift in the equilibrium position.

4 Results

4.1 Electronic spectra in gas phase

4.1.1 DSB S_0 and S_1 PESs

Preliminary calculations were carried out at QM level on the isolated DSB dye, for a first description of the most important features of both the S_0 and the S_1 potential energy surfaces (PESs). The bright state corresponds to a $\pi\pi^*$ transition [80], essentially described by a HOMO$\rightarrow$ LUMO excitation (for a discussion on the quasi mono-configurational character of the $S_0 \rightarrow S_1$ transition, see Ref [81]), which is characterized by a notable shift in electron density from the double C=C bond within the vinylene unit towards the neighbouring single bonds (see Figure S8 in the SI). Consequently, there is a reduction of the bond order for double bonds and an increase of the bond order for single bonds, with a slightly greater effect on the inner C-C bond. This redistribution has a direct impact on the corresponding C-C distances in the ground and excited states, which are summarized in Table S12 in the SI for various DFT functionals such as CAM-B3LYP, PBE0, M06-2X, ωB97XD, and M11. Notably, the most significant change in bond length (shortening) is observed for the inner C-C bond, aligning with the electronic redistribution upon electronic excitation. Among the functionals compared, PBE0 exhibits smaller changes, while CAM-B3LYP, M06-2X, and ωB97XD have similar behavior, with slightly larger changes observed for the latter functional. Finally, M11 yields the most pronounced alterations in bond distances.

Furthermore, the electron density redistribution also affects the energy profile around the torsion of the single C-C bonds within the vinylene units. As depicted in Figure 4, the profiles of the single bonds in the S_0 state (i.e., δ_1 and δ_2 torsions, displayed in the inset) become more rigid in the excited state. [46] This effect remains consistent across all functionals, exhibiting a relatively flat profile around the minimum in the ground state, which becomes considerably

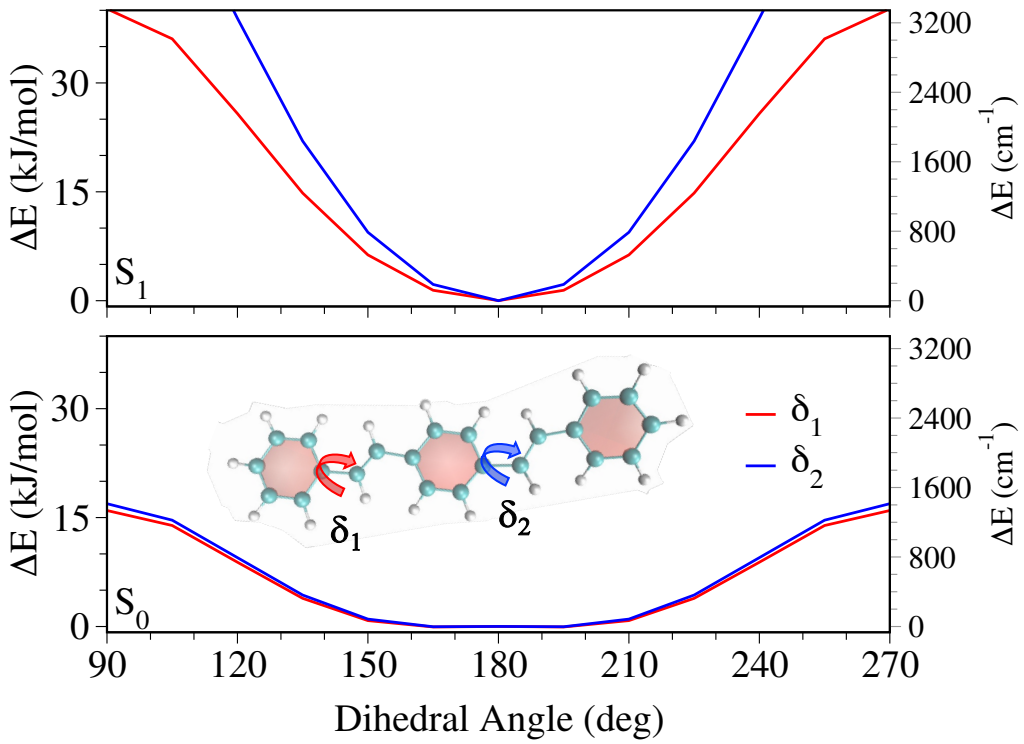

Figure 4: Energy profiles over the torsions δ_1 (red lines),δ_2 (blue lines) around single C-C bonds, evidenced in the inset, in the ground (S_0, bottom panel) and excited (S_1, upper panel) states computed with CAM-B3LYP (results for other functionals are included in Figure S9 in the SI).

stiffer in the excited states. Both torsions, δ_1 and δ_2, are characterized by similar profiles, particularly in the ground state. In the excited state, the profile for δ_2 features higher barriers, further corroborating the electronic redistribution associated with the HOMO→LUMO transitions. Similar trends are observed for all investigated functionals, with ωB97XD showing slightly larger barriers at $\delta = 180$ degrees (see Figure S9).

4.1.2 Static vibronic spectra

To first ascertain the accuracy of the investigated DFT functionals in reproducing the high-resolution features of the experimental signals, absorption and emission spectra were computed for the isolated dye and compared with those obtained experimentally [46] at low temperature

(10K) in a weakly interacting solvent as EPA. Such preliminary tests were also carried out to gain a deeper insight on the effect of the most flexible coordinates on the resulting spectral shape. In consideration of the scarce effect exerted by the simple solvent on the dye's structure, all spectra at this stage were computed with a so-called "static" approach, where no statistical sampling from MD runs is required. Moreover since δ_1 and δ_2 torsions are predicted to have extremely small vibrational frequencies (0.06 cm^{-1} for CAM-B3LYP), their contribution was initially neglected, by projecting them out from the vibrational space, as it will later be discussed in detail.

The top panels of Figure 5 display the lineshapes obtained with the VH model for the CAM-B3LYP functional, showing it performs excellently for emission and still acceptably for absorption. Moreover, Figure S10 in the SI shows that M06-2X, and ωB97XD functionals perform similarly well, whereas PBE0 and M11 demonstrate deviations, with PBE0 showing a too-short progression, and M11 displaying, on the contrary, a too-large one. These discrepancies can be attributed to the change in C-C distances from the ground state to the excited state, which is too small for PBE0 and too large for M11. Overall, CAM-B3LYP shows the closest agreement with the experiment and, unless otherwise stated, all QMD-FF and Ad-MD|gVH calculations were performed with this functional. Although we neglected the contribution of δ_1 and δ_2, it is however clear that it is expected to be remarkable, especially in absorption. In order to show this, we re-introduced such degrees of freedom in the spectra reported in the bottom panels of Figure 5. This required to adopt the AH vibronic model. In fact, some imaginary frequencies associated to the torsions arise at the FC point in the VH approach (due to their strongly anharmonic energy profile), whereas vibrational frequencies are by definition all real in the AH approach which expands the PESs at the minima of the initial and final states. The large broadening at 10 K obtained with the full coordinate space confirms that the torsion have an impact on the spectral shape in especially in absorption. Being remarkably overestimated with respect to experiment, such broadening also indicates that the description of the torsions at harmonic level is strongly inaccurate. This was expected since the flat potentials shown in Figure 4 cannot be approximated with a harmonic expansion. The effect of such inaccuracy will become even more relevant at room temperature, where the conformational space accessible to the flexible

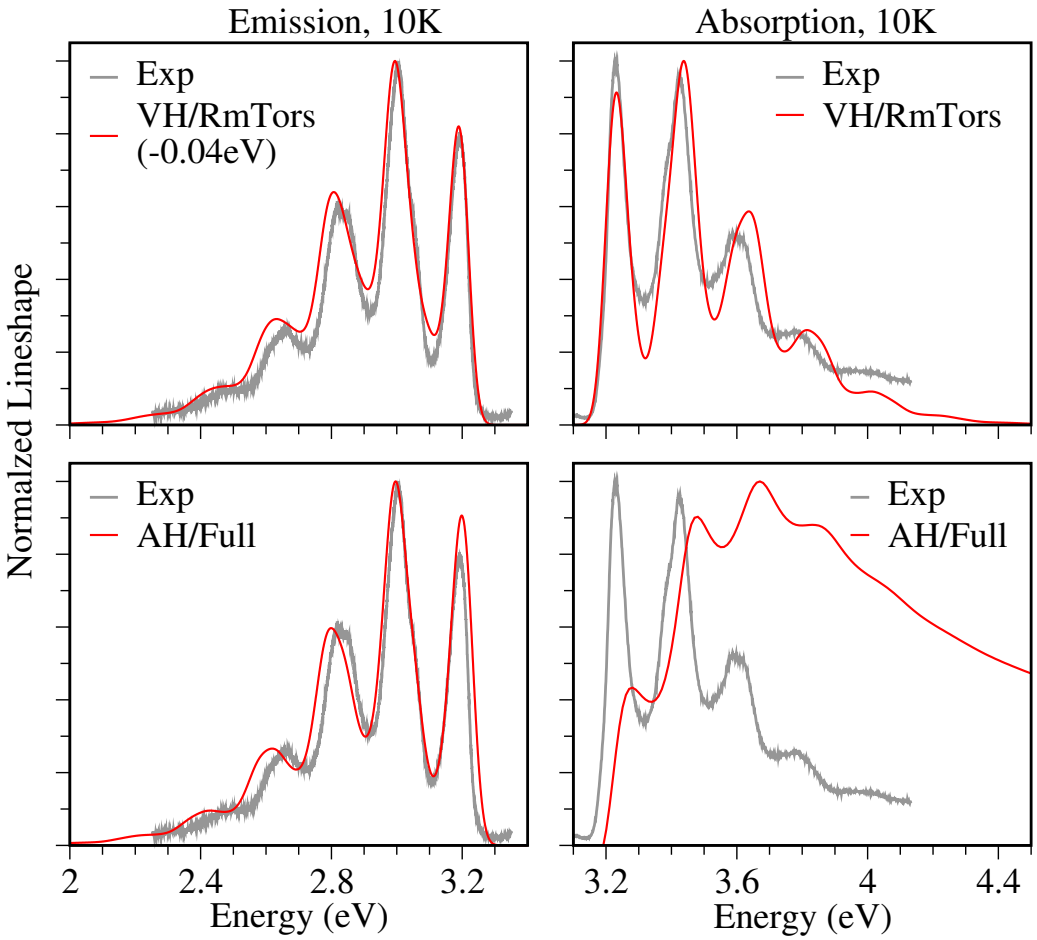

Figure 5: Absorption and emission spectra lineshapes in the gas phase at 10 K computed with the VH model projecting out the torsions δ_1 and δ_2 from the vibrational space (top panels) or retaining the full space (bottom panels). The spectra are broadened with a Gaussian profile having HWHM=0.03 eV. It is worth noticing that this value, here introduced phenomenologically for these preliminary computations, can be determined more rationally, as discussed in sections C.4 and D.2.1 of the SI. When required, the simulations were shifted (by the amount indicated in the figure) to better match the experimental spectra (grey lines), measured at 10 K in EPA ad taken from ref. [47]

coordinates further deviates from the one expected by a harmonic approximation.

Figure 6 displays as lineshapes both the experimental spectra, measured in EPA at low and room temperatures, and those computed in an AH model accounting for all coordinates (including torsions). The simulated absorption spectra, especially at room temperature, clearly exhibit excessive broadening when compared to the experimental results. Such remarkable

effect can be traced back to the extremely low frequencies obtained for the torsional modes, with a value as low as 0.06 cm^{-1}. As shown in the SI, Figure S11, the effect significantly depends on the functional, and it is not perceptible with PBE0 at 10 K, since this functional predicts a larger frequency for this torsional mode (4.5 cm^{-1}). It is worth noting that, although to a lesser extent, the experimental spectra at 10 K also exhibit an asymmetry between absorption and emission, with the absorption bands appearing broader, a behavior again consistent with the flatter potential energy profile in the S_0 state.

In conclusion, the preliminary static spectra confirm that, on the one hand, the presence of such a flat potential presents a challenge when relying on the harmonic approximation, hence leading to artefacts and inaccurate absorption bands. On the other hand, the contribution of

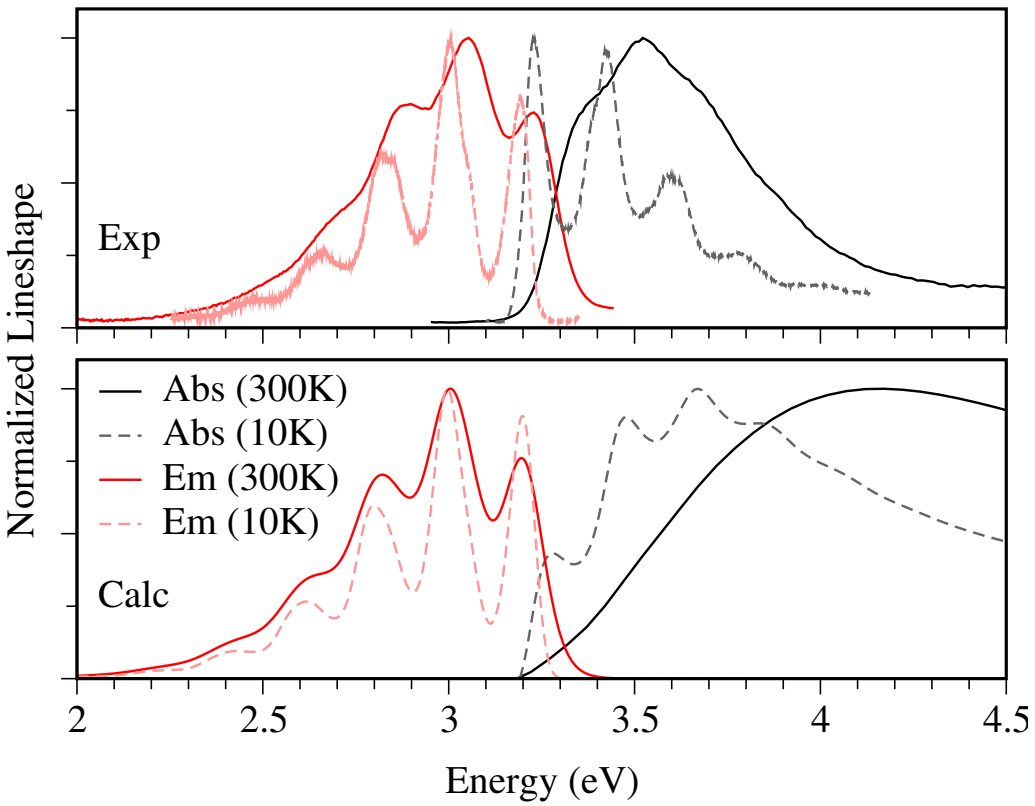

Figure 6: Absorption and emission spectra lineshapes at 10 and 300 K, experimentally measured in EPA (top panel), [47] or computed in the gas phase without projecting out the torsions δ_1 and δ_2 from the vibrational space (bottom panel). All computed spectra are broadened with a Gaussian profile having HWHM=0.03 eV.

such torsions to the observed lineshape is non-negligible, particularly in absorption, and should be correctly included in the calculations.

The flatness of the torsional potential causes a significant sensitivity of DSB's conformational dynamics to the interaction established with the embedding environment, since both the shape and the low energy barriers of the torsional profiles can be remarkably altered by the presence of different surrounding frameworks. It is therefore evident that such combined effect prevents the straightforward application of simple static approaches, whereas, on the contrary, both DSB structural flexibility and its consequent responsiveness to varied environments call for more accurate and multi-level approaches, as the Ad-MD|gVH protocol, whose results are discussed in detail in the next sections. Before closing this section, it is worth noticing that earlier works by some of us [46, 82] have documented that the effect of the flexible torsions in the absorption of DSB can be actually recovered by convoluting the contribution of the vibronic bands of the stiff (in-plane) modes (taken as the mirror-image of the experimental emission), with classical exponential distributions arising from the relative change of the curvature of the ground and excited energy profiles (treated in that case as a phenomenological parameter). This approach, relies on conditions for the separability of these modes, [82] and provides an easy route to account for the torsions effect, and in fact similar computations have been reported also for trans-stilbene [14, 46]. Being based on experimental data and spectra, it follows a different philosophy from the fully first-principle approach we are pursuing here, which has the goal to describe microscopically the effect of the environment on these vibrations. Notwithstanding this, the success of those results suggests that the overestimation of the broadening in our computations can be not only due to the lack of anharmonic effects but also to the (related) underestimation of the S_0 torsional frequencies predicted by CAM-B3LYP at harmonic level. This consideration highlights limits of the accuracy of the currently available electronic structure methods, which will be further discussed below. We finally mention that the use of classical distributions to account for the contributions of torsions, assuming they are not not-coupled with the other degrees of freedom, has been also explored for anharmonic energy profiles in ref. [83] and ref. [69]. As we will discuss later in Section 4.2.2, this approach was also adopted in the present work (sections C4 and D2.1 of the SI) to analyse in a simple way the connection

between the computed QM torsional profiles and the residual inaccuracies in the absorption spectra predicted with our Ad-MD|gVH approach.

4.2 Electronic spectra in complex environments

4.2.1 QMD-FFs parameterization and MD simulations

As a first step for the application of the Ad-MD|gVH approach, it is necessary to parameterize a QMD-FF for DSB's ground and excited state, as described in the following. The intramolecular term of the QMD-FF is derived against the reference CAM-B3LYP/6-31+G(d,p) data, computed for the isolated target molecule at DFT or TD-DFT level for S_0 and S_1, respectively. The usual partition [56, 58] of energy contributions is applied to build the energy expression of the QMD-FF intramolecular contribution (E^{FF}_{intra}) in terms of internal coordinates, bonds (**b**), angles (**a**), dihedrals (stiff $\mathbf{d}^s$ and flexible $\mathbf{d}^f$) and non-bonded atom pairs (**p**) (see also Section A in the SI).

$$E^{QMD-FF}_{intra}(\{\mathbf{b},\mathbf{a},\mathbf{d},\mathbf{p}\}) = E_s(\mathbf{b}) + E_b(\mathbf{a}) + E_{st}(\mathbf{d}^s) + E_{ft}(\mathbf{d}^f) + E_{Nb}(\mathbf{p}) \quad (1)$$

where terms for bonds (E_s), angles (E_b) and stiff dihedrals (E_{st}) are described with harmonic expressions, those of flexible torsions (E_{ft}) with a Fourier-like expression. Non-bonded intramolecular terms (E_{Nb}) are usually described with Coulomb and Lennard-Jones potentials. We note, however, that in this case, no non-bonded term was included in the intramolecular QMD-FF. The same analytical expression is adopted for both S_0 and S_1 PESs. In order to assess the quality of the intra-molecular parameterizations, we compared key features of the QM PES with the MM potential using the developed QMD-FF. As displayed in Figure S3 of the SI, for each state the QMD-FF is able to well describe both the fast oscillations of the stiff modes around the equilibrium structure and the behaviour of the more flexible coordinates, while spanning larger portions of the isolated chromophore's PES. All the resulting intermolecular QMD-FF parameters for DSB are reported in detail in the SI. Turning to the QMD-FF intermolecular term, consistently with the two environments, LJ parameters were straightforwardly transferred from OLPS-AA [84], whereas, to account for the specificity of each embedding, the DSB point charges were derived for each state, based on the computed electronic density of the dye embedded at PCM level in a continuous medium with a proper electric constant (dodecane for

n-tetradecene and cyclohexane for PHTP).

MD simulations were carried out with the resulting QMD-FF at 300 K with DSB either in vacuo, dispersed in tetradecane or inserted into a PHTP matrix. As the flexible dihedrals were found to play an essential role in tuning the spectral features, a first analysis was carried out by monitoring their behaviour along the S_0 and S_1 trajectories in the different environments, and the resulting populations are displayed in Figure 7. Simulations in gas and in tetradecane

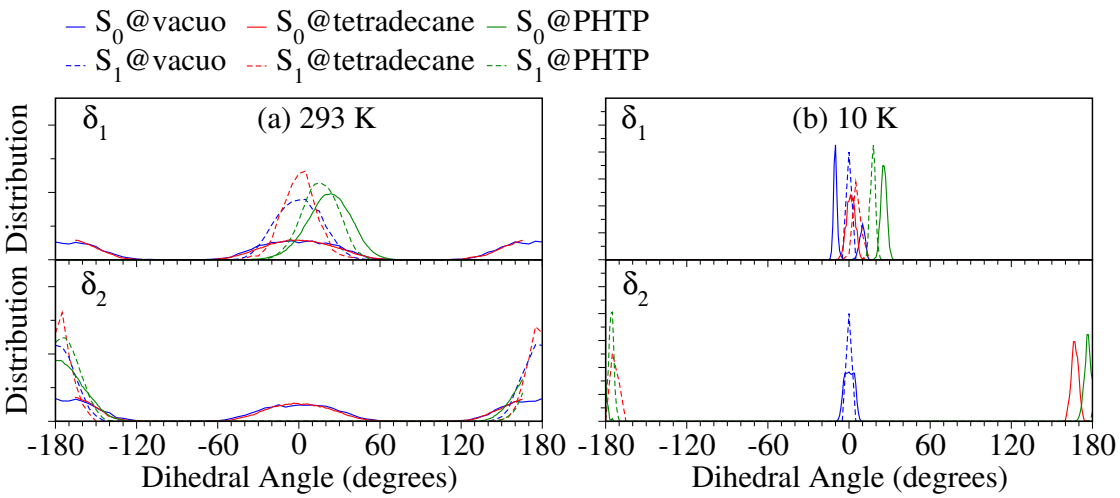

Figure 7: Distribution of flexible (δ, around σ C-C bonds) dihedrals of DSB molecule in its ground and excited state during the MD run performed on the isolated molecule and embedded in the considered environments (tetradecane and PHTP) both (a) at 300 K and (b) at 10 K.

lead to similar behavior. Namely, in S_0, both flexible dihedrals, δ_1 and δ_2, sample the two degenerate minima at 0° and 180° , showing a wide distribution around each planar conformer. In S_1, on the contrary, only one between these conformers is populated, evidencing how DSB conformational dynamics is hampered by the larger barriers found in the excited state for both δ_1 and δ_2 dihedrals. The scenario changes significantly in PHTP, where DSB flexible dihedrals get trapped in a non-planar conformation, to better fit the dye onto the pseudohexagonal nanochannels formed by the supramolecular network of PHTP units. Such environmental constraints not only block the torsions but also displace their average position, breaking the planarity, especially for δ_1, in both S_0 and S_1. This shift is slightly larger for S_0, consistently with the larger

flatness of the potential of this state. When the temperature is lowered to 10 K, all dihedrals get trapped at the initial configuration. There are, however, some differences in the actual position for each embedding. Namely, while gas phase simulation populates the two non-planar wells symmetric with respect to the planar configuration that are observed in the flat DFT S_0 potential, in the case of tetradecane, the alkyl chains restrain the dihedrals around planar configurations in S_0. In both the gas phase and tetradecane, simulations at S_1 populate the planar configuration. The situation with PHTP shows again a shift olong δ_1, which is more pronounced at S_0, but still noticeable also at S_1.

4.2.2 Computation of the spectral shapes in complex environments with Ad-MD|gVH

Once verified that the MD simulations account for the different constraining effects exerted by the varied environments on DSB's flexibility and conformational dynamics, we now investigate up to what extent the Ad-MD|gVH protocol is able to reproduce how such features reflect on the shape of the electronic spectra. It is worth noticing that, since in the previous figures we have documented that absorption and emission spectra are far from being mirror-symmetric even when plotted as lineshapes, for a more straightforward comparison with the experimental spectra displayed in the original papers, [46,47] in the following we report emission spectra as intensities. The spectra computed at room temperature (293 K) are compared with their experimental counterparts in Figure 8. The experimental trend is clearly reproduced: in agreement with the experiment, the effect on the spectral shape of a simple low-mass weight solvent mixture (EPA), here approximated to gas phase calculations, or of a long saturated hydrocarbon (*n*-tetradecane), is comparable and leads in absorption to a similar unstructured band shape. Additionally, our method nicely reproduces the fact that limitations to the flexibility of the molecule imposed by the tubular organization of the PHTP have a remarkable impact on absorption spectra, which are narrower and characterized by a much better resolved vibronic structure. Finally, again in line with the experimental trends, the emission band shapes are always very well resolved and quite similar in all environments.

Figure 9 reports both the experimental and simulated spectra at temperatures as low as 10 K. At such ultra-cold conditions, the band shapes, for emission and for absorption, become

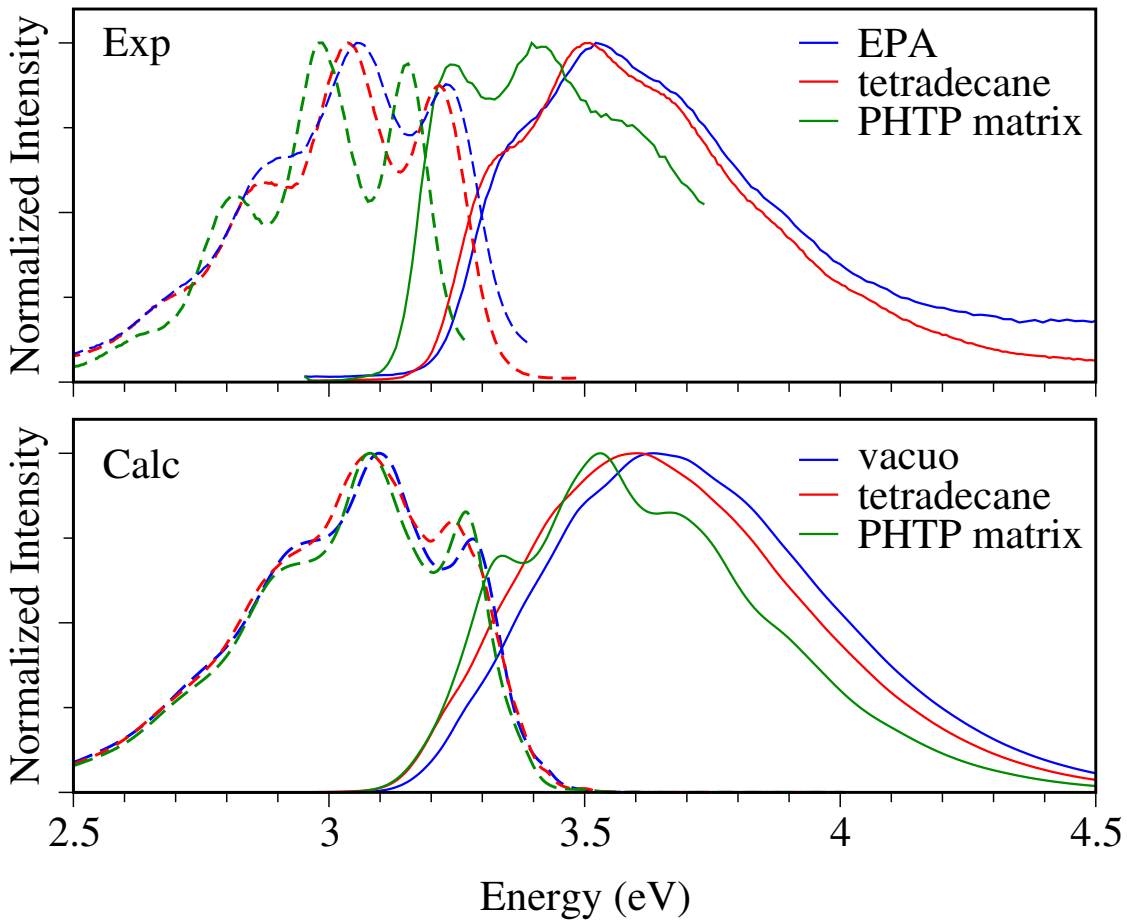

Figure 8: Experimental (top) and Ad-MD|gVH computed (bottom) absorption (solid lines) and emission (dashed lines) spectra for the DSB molecule in different environments at 293 K and 1 atm. Experimental data taken from [47].

very similar in both *n*-tetradecane and PHTP matrix. In these conditions, the contribution of the torsion is nearly suppressed, thus rendering all lineshapes extremely similar. Despite the ultra-low temperature regime might challenge the application of the classical approximation, also in this case, our mixed quantum-classical protocol is able to reproduce such an effect, recovering the vibrational structure also in the *n*-tetradecane case. It is interesting to notice that our calculations also capture the fact that at low temperatures, while the position of the emission spectra is coincident in PHTP and tetradecane, the absorption in PHTP is slightly blue-shifted with respect to the one in tetradecane (Figure 9). The distributions of the dihedral δ_1 in Figure 7 provide a rationale for this finding, showing that in PHTP δ_1 is frozen at values $\sim$30 degrees,

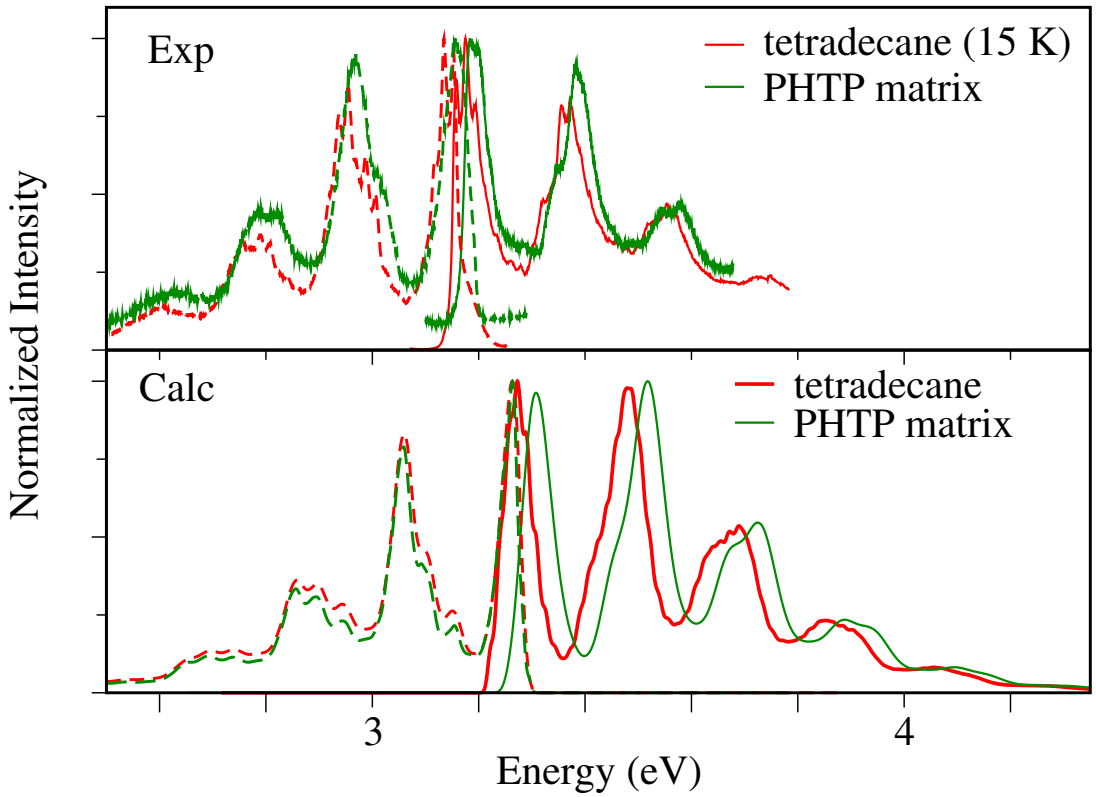

Figure 9: Experimental (top) and Ad-MD|gVH computed (bottom) absorption (solid lines) and emission (dashed lines) spectra for the DSB molecule in different environments at 10 K and 1 atm. Experimental data taken from [47].

while it peaks at 0 degrees in tetradecane. Since the potential along δ_1 is steeper on S_1 than on S_0 this leads to a blue-shift of the $S_0 \rightarrow S_1$ vertical transition.

In order to provide an overall picture of the simulation of the temperature effect, Figure 10 compares the absorption spectra of DSB, experimentally registered [46, 47] at high (293K) and low (15/10K) temperatures in *n*-tetradecane and PHTP respectively with those computed by means of the Ad-MD|gVH procedure in the same thermodynamic conditions. It is apparent that in both environments the method is capable of reproducing the insurgence of the vibronic structure decreasing the temperature. Therefore, besides the effect of the embedding environment, our computational approach seems to succeed in accounting for the large variations arising in the spectral shape upon cooling to ultra-low temperatures.

Despite the very encouraging replication of the experimental trends, the computed absorp-

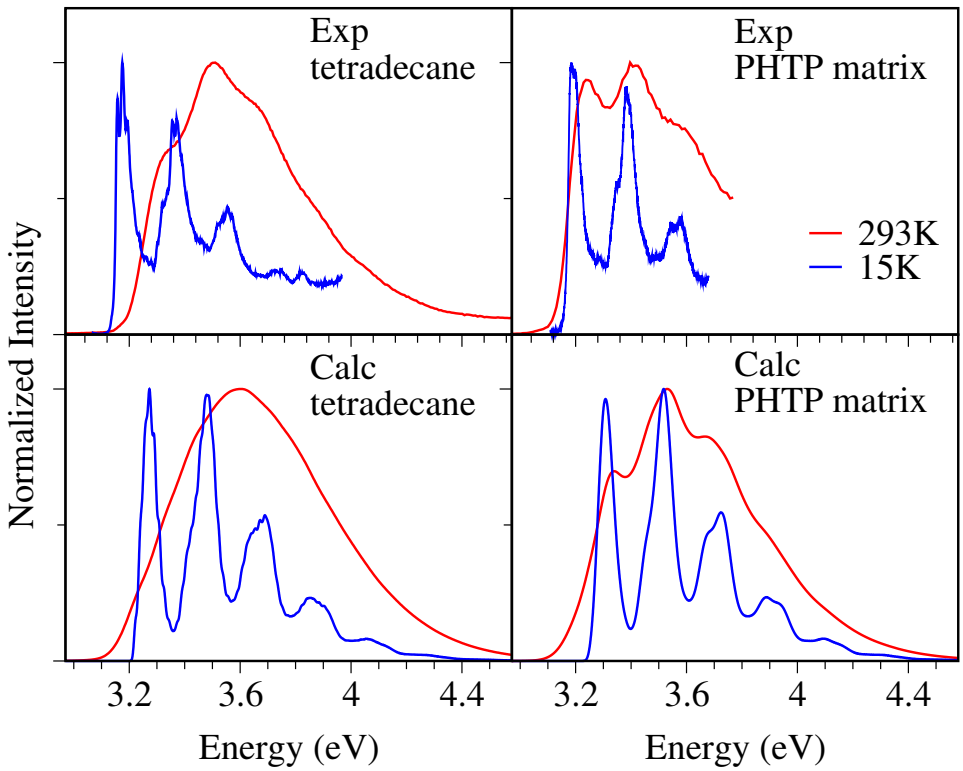

Figure 10: Experimental (top) and Ad-MD|gVH computed (bottom) absorption spectra for the DSB molecule solvated in *n*-tetradecane(left) or inserted in a PHTP matrix (right) at different temperatures and 1 atm. Experimental data taken from [47].

tion spectra at room temperature are, in general, too broad with respect to the experimental counterparts. In Section D of the SI we use simplified approaches to analyse in detail the cause of this discrepancy, documenting that it is directly linked to inaccuracies in the computed QM energy profiles for the flexible torsions δ_1 and δ_2. We also show test computations moving from DFT to post-HF methods like MP2/ADC(2).

5 Conclusions

In this work we have shown that our recently proposed mixed quantum-classical approach Ad-MD|gVH effectively captures the experimental trends observed in the shape of absorption and emission bands of DSB immersed in different embeddings at varied thermodynamic conditions.

In particular we reproduce the narrower and more well-defined vibrational features observed when introducing the molecule into a PHTP matrix. The ability to tune the spectral shape by altering the environment highlights the interplay between torsions of rotatable bonds of the dye and environmental constraints, making this system ideal for investigating the performance of protocols to simulate photophysics in complex environments. In particular, Ad-MD|gVH explains the limited effect induced by a disordered alkane solvent, *n*-tetradecane, where the DSB absorption spectrum is broad, similar to that in a low-molecular-weight solvent, such as EPA. In contrast, the channel-forming host, PHTP, limits the solute conformational dynamics along the single-bond torsions with a large impact on the spectrum, drastically reducing the broadening, and resulting in a well-resolved structure.

The effect of ultra-cold temperatures is also nicely captured by our methods. As expected, the spectra become much more well-resolved in all environments. Moreover, the constraints imposed by PHTP, perturbs the equilibrium structure, both in S_0 and S_1, breaking the planarity. As a result, the ultra-cold spectrum of PHTP is significantly blue-shifted, since the transition energy increases as we deviate from planarity due to the steep increase in S_1 energy. Such an effect is clearly observed in the experiment, where both absorption and emission spectra at room temperature appear at lower energies compared to those in tetradecane, while the scenario at 10 K is reversed, with the spectrum in PHTP appearing at higher energies. Nonetheless, even if the application of our method to low temperatures was successful, it should be warned that it implies the description of torsions classically, which is questionable at such ultra-cold conditions. In this sense, a potential improvement of the protocol would involve replacing the classical MD sampling by a method able to provide the correct QM sampling, such as Path Integral MD [85].

Despite nicely reproducing the experimental trends, the predicted spectral shapes in absorption still show some discrepancies with respect to the experimental counterparts, since they are broader and underestimate the relative intensity of the 0-0 band. Our analysis allows to attribute these discrepancies to the limited accuracy electronic level of theory, i.e. DFT/TDF-DFT with CAM-B3LYP functional. Computations with MP2/ADC(2) protocol improves the results but only partially highlighting that, at the state-of-the-art, it can be quite challenging finding a first-

principle level of theory able to accurately describe the balance between internal flexibility and the limitations due to the steric hindrance of the environment.

In summary, our methodology demonstrates good agreement with experimental observations, providing valuable insights into the distinct influence of different complex environments on the photophysics of a flexible system. The method shows promise in capturing essential spectral characteristics and provides a valuable framework to approach flexible systems in complex environments, and is envisaged for the study of systems with relevant biological and technological implications, such as bioluminescent proteins or advanced devices for solar energy conversion.

Acknowledgments

F.S. and G.P. thank the support of ICSC - Centro Nazionale di Ricerca in High Performance Computing, Big Data and Quantum Computing, funded by European Union - NextGenerationEU - PNRR, Missione 4 Componente 2 Investimento 1.4. J.G. acknowledges funding by the Spanish Ministerio de Ciencia e Innovación (MICIN-FEDER project PID2022-138222NB-C21), by the Severo Ochoa program for Centers of Excellence in R&D of the MICIN (CEX2020-001039-S), and by the Campus of International Excellence (CEI) UAM+CSIC. J.C. thanks Ministerio de Universidades, Plan de Recuperación, Transformación y Resiliencia and UAM for funding the research stay in Pisa with a requalification program (CA2/RSUE/2021-00890) and the MICINN Project PID2019-110091GB-I00 for financial support. Computational resources provided by ICCOM and the Centro de Cálculo Científico at Universidad Autónoma de Madrid (CCC-UAM) are also acknowledged.

References

[1] Mateo-Alonso, A. π-Conjugated Materials: Here, There, and Everywhere *Chem. Mater.* **2023**, *35*, 1467–1469.

[2] Gierschner, J.; Shi, J.; Milián-Medina, B.; Roca-Sanjuán, D.; Varghese, S.; Park, S. Luminescence in Crystalline Organic Materials: From Molecules to Molecular Solids *Advanced Optical Materials* **2021**, *9*, 2002251.

[3] Zollinger, H. Color Chemistry: Syntheses, Properties, and Applications of Organic Dyes and Pigments; Weinheim: VCH, 1991.

[4] Ha, J. M.; Hur, S. H.; Pathak, A.; Jeong, J.-E.; Woo, H. Y. Recent advances in organic luminescent materials with narrowband emission *NPG Asia Materials* **2021**, *13*.

[5] Eskandari, M.; Roldao, J. C.; Cerezo, J.; Miliá-Medina, B.; Gierschner, J. Counterion-Mediated Crossing of the Cyanine Limit in Crystals and Fluid Solution: Bond Length Alternation and Spectral Broadening Unveiled by Quantum Chemistry *Journal of the American Chemical Society* **2020**, *142*, 2835–2843; PMID: 31957436.

[6] Linne, M. A. Spectroscopic measurement : an introduction to the fundamentals; Academic Press, 2002.

[7] Tomasi, J.; Mennucci, B.; Cammi, R. Quantum Mechanical Continuum Solvation Models *Chem. Rev.* **2005**, *105*, 2999–3094.

[8] Mennucci, B.; Cappelli, C.; Guido, C. A.; Cammi, R.; Tomasi, J. Structures and Properties of Electronically Excited Chromophores in Solution from the Polarizable Continuum Model Coupled to the Time-Dependent Density Functional Theory *J. Phys. Chem. A* **2009**, *113*, 3009–3020.

[9] Charaf-Eddin, A.; Planchat, A.; Mennucci, B.; Adamo, C.; Jacquemin, D. Choosing a Functional for Computing Absorption and Fluorescence Band Shapes with TD-DFT *J. Chem. Theory Comput.* **2013**, *9*, 2749–2760.

[10] Avila Ferrer, F. J.; Cerezo, J.; Soto, J.; Improta, R.; Santoro, F. First-principle computation of absorption and fluorescence spectra in solution accounting for vibronic structure, temperature effects and solvent inhomogenous broadening *Comput. Theoret. Chem.* **2014**, *1040–1041*, 328–337.

[11] Santoro, F.; Jacquemin, D. Going Beyond the Vertical Approximation with TD-DFT *WIREs Comput. Mol. Sci.* **2016**, *6*, 460–486.

[12] Dierksen, M.; Grimme, S. An efficient approach for the calculation of Franck–Condon integrals of large molecules *J. Chem. Phys.* **2005**, *122*, 244101.

[13] Hazra, A.; Nooijen, M. Derivation and Efficient Implementation of a Recursion Formula to Calculate Harmonic Franck-Condon Factors for Polyatomic Molecules *Int. J. Quantum Chem.* **2003**, *95*, 643–657.

[14] Santoro, F.; Improta, R.; Lami, A.; Bloino, J.; Barone, V. Effective method to compute Franck-Condon integrals for optical spectra of large molecules in solution *J. Chem. Phys.* **2007**, *126*, 084509.

[15] Santoro, F.; Lami, A.; Improta, R.; Bloino, J.; Barone, V. Effective method for the computation of optical spectra of large molecules at finite temperature including the Duschinsky and Herzberg–Teller effect: The Qx band of porphyrin as a case study *J. Chem. Phys.* **2008**, *128*, 224311.

[16] Jankowiak, H.-C.; Stuber, J. L.; Berger, R. Vibronic transitions in large molecular systems: Rigorous prescreening conditions for Franck-Condon factors *J. Chem. Phys.* **2007**, *127*, 234101.

[17] Tang, J.; Lee, M. T.; Lin, S. H. Effects of the Duschinsky mode-mixing mechanism on temperature dependence of electron transfer processes *J. Chem. Phys.* **2003**, *119*, 7188–7196.

[18] Ianconescu, R.; Pollak, E. Photoinduced Cooling of Polyatomic Molecules in an Electronically Excited State in the Presence of Dushinskii Rotations *J. Phys. Chem. A* **2004**, *108*, 7778–7784.

[19] Tatchen, J.; Pollak, E. Ab initio spectroscopy and photoinduced cooling of the trans-stilbene molecule *J. Chem. Phys.* **2008**, *128*, 164303.

[20] Lami, A.; Santoro, F. Time-Dependent Approaches to Calculation of Steady-State Vibronic Spectra: From Fully Quantum to Classical Approaches; John Wiley & Sons, Inc., 2011; Chapter 10, pp 475–516.

[21] Vendrell, O.; Meyer, H.-D. Multilayer multiconfiguration time-dependent Hartree method: Implementation and applications to a Henon-Heiles Hamiltonian and to pyrazine *J. Chem. Phys.* **2011**, *134*, 044135.

[22] Worth, G. Quantics: A general purpose package for quantum molecular dynamics simulations *Comput. Phys. Commun.* **2020**, *248*, 107040.

[23] Köppel, H.; Domcke, W.; Cederbaum, L. In *Conical Intersections, Electronic Structure, Dynamics and Spectroscopy*; World Scientific Publishing Co. Singapore; pp 323–368.

[24] Aranda, D.; Santoro, F. Vibronic spectra of π-conjugated systems with a multitude of coupled states: A protocol based on linear vibronic coupling models and quantum dynamics tested on hexahelicene *J. Chem. Theory Comput.* **2021**, *17*, 1691–1700.

[25] Segalina, A.; Aranda, D.; Green, J. A.; Cristino, V.; Caramori, S.; Prampolini, G.; Pastore, M.; Santoro, F. How the Interplay among Conformational Disorder, Solvation, Local, and Charge-Transfer Excitations Affects the Absorption Spectrum and Photoinduced Dynamics of Perylene Diimide Dimers: A Molecular Dynamics/Quantum Vibronic Approach *J. Chem. Theory Comput.* **2022**, *18*, 3718–3736.

[26] D'Abramo, M.; Aschi, M.; Amadei, A. Theoretical modeling of UV-Vis absorption and emission spectra in liquid state systems including vibrational and conformational effects: Explicit treatment of the vibronic transitions *J. Chem. Phys.* **2014**, *140*, 164104.

[27] Cerezo, J.; Ferrer, F. J. A.; Prampolini, G.; Santoro, F. Modeling Solvent Broadening on the Vibronic Spectra of a Series of Coumarin Dyes. From Implicit to Explicit Solvent Models *J. Chem. Theory Comput.* **2015**, *11*, 5810–5825.

[28] Loco, D.; Cupellini, L. Modeling the absorption lineshape of embedded systems from molecular dynamics: A tutorial review *Int. J. Quantum Chem.* **2019**, *119*, e25726.

[29] Zuehlsdorff, T. J.; Isborn, C. M. Modeling absorption spectra of molecules in solution *Int. J. Quantum Chem.* **2019**, *119*, e25719.

[30] Zuehlsdorff, T. J.; Montoya-Castillo, A.; Napoli, J. A.; Markland, T. E.; Isborn, C. M. Optical spectra in the condensed phase: Capturing anharmonic and vibronic features using dynamic and static approaches *J. Chem. Phys.* **2019**, *151*, 074111.

[31] Mukamel, S. Fluorescence and absorption of large anharmonic molecules - spectroscopy without eigenstates *The Journal of Physical Chemistry* **1985**, *89*, 1077–1087.

[32] Valleau, S.; Eisfeld, A.; Aspuru-Guzik, A. On the alternatives for bath correlators and spectral densities from mixed quantum-classical simulations *The Journal of Chemical Physics* **2012**, *137*, 224103.

[33] Jang, S. J.; Mennucci, B. Delocalized excitons in natural light-harvesting complexes *Rev. Mod. Phys.* **2018**, *90*, 035003.

[34] Bondanza, M.; Nottoli, M.; Cupellini, L.; Lipparini, F.; Mennucci, B. Polarizable embedding QM/MM: the future gold standard for complex (bio)systems? *Phys. Chem. Chem. Phys.* **2020**, *22*, 14433–14448.

[35] Allan, L.; Zuehlsdorff, T. J. Taming the third order cumulant approximation to linear optical spectroscopy *The Journal of Chemical Physics* **2024**, *160*, 074108.

[36] Cerezo, J.; Aranda, D.; Avila Ferrer, F. J.; Prampolini, G.; Santoro, F. Adiabatic-Molecular Dynamics Generalized Vertical Hessian Approach: A Mixed Quantum Classical Method to Compute Electronic Spectra of Flexible Molecules in the Condensed Phase *J. Chem. Theory Comput.* **2020**, *16*, 1215–1231.

[37] Segalina, A.; Cerezo, J.; Prampolini, G.; Santoro, F.; Pastore, M. Accounting for Vibronic Features through a Mixed Quantum-Classical Scheme: Structure, Dynamics, and Absorption Spectra of a Perylene Diimide Dye in Solution *J. Chem. Theory Comput.* **2020**, *16*, 7061–7077.

[38] Cerezo, J.; Gao, S.; Armaroli, N.; Ingrosso, F.; Prampolini, G.; Santoro, F.; Ventura, B.; Pastore, M. Non-Phenomenological Description of the Time-Resolved Emission in Solution with Quantum-Classical Vibronic Approaches. Application to Coumarin C153 in Methanol *Molecules* **2023**, *28*, 3910.

[39] Gierschner, J.; Lüer, L.; Milián-Medina, B.; Oelkrug, D.; Egelhaaf, H.-J. Highly Emissive H-Aggregates or Aggregation-Induced Emission Quenching? The Photophysics of All-Trans para-Distyrylbenzene *The Journal of Physical Chemistry Letters* **2013**, *4*, 2686–2697.

[40] Shi, J.; Aguilar Suarez, L. E.; Yoon, S.-J.; Varghese, S.; Serpa, C.; Park, S. Y.; Lüer, L.; Roca-Sanjuán, D.; Milián-Medina, B.; Gierschner, J. Solid State Luminescence Enhancement in π-Conjugated Materials: Unraveling the Mechanism beyond the Framework of AIE/AIEE *The Journal of Physical Chemistry C* **2017**, *121*, 23166–23183.

[41] Nguyen, D. D.; Jones, N. C.; Hoffmann, S. V.; Spanget–Larsen, J. Near and vacuum UV polarization spectroscopy of 1,4-distyrylbenzene *Spectrochimica Acta Part A: Molecular and Biomolecular Spectroscopy* **2023**, *286*, 122019.

[42] Egelhaaf, H.-J.; Brun, M.; Reich, S.; Oelkrug, D. Luminescence and photoconductivity studies on bonding, mobility and electronic deactivation in submonolayers and thin films of Distyrylbenzene *Journal of Molecular Structure* **1992**, *267*, 297–302; MOLECULAR SPECTROSCOPY AND MOLECULAR STRUCTURE 1991 Proceedings of the XXth European Congress on Molecular Spectroscopy.

[43] Gierschner, J.; Lüer, L.; Oelkrug, D.; Musluoğlu, E.; Behnisch, B.; Hanack, M. Preparation and Optical Properties of Oligophenylenevinylene/Perhydrotriphenylene Inclusion Compounds *Advanced Materials* **2000**, *12*, 757–761.

[44] Gierschner, J.; Lüer, L.; Oelkrug, D.; Musluoğ, E.; Behnisch, B.; Hanack, M. One dimensional coupling of oligophenylenevinylenes in perhydrotriphenylene matrices *Synthetic Metals* **2001**, *121*, 1695–1696; Proceedings of the International Conference on the Science and Technology of Synthetic Metals.

[45] Poulsen, L.; Jazdzyk, M.; Communal, J.-E.; Sancho-García, J. C.; Mura, A.; Bongiovanni, G.; Beljonne, D.; Cornil, J.; Hanack, M.; Egelhaaf, H.-J.; Gierschner, J. Three-Dimensional Energy Transport in Highly Luminescent Host-Guest Crystals: A Quantitative Experimental and Theoretical Study *Journal of the American Chemical Society* **2007**, *129*, 8585–8593; PMID: 17564450.

[46] Gierschner, J.; Mack, H.-G.; Lüer, L.; Oelkrug, D. Fluorescence and absorption spectra of oligophenylenevinylenes: Vibronic coupling, band shapes, and solvatochromism *J. Chem. Phys.* **2002**, *116*, 8596–8609.

[47] Srinivasan, G.; Villanueva-Garibay, J. A.; Müller, K.; Oelkrug, D.; Milian Medina, B.; Beljonne, D.; Cornil, J.; Wykes, M.; Viani, L.; Gierschner, J.; Martinez-Alvarez, R.; Jazdzyk, M.; Hanack, M.; Egelhaaf, H. J. Dynamics of guest molecules in PHTP inclusion compounds as probed by solid-state NMR and fluorescence spectroscopy *Phys. Chem. Chem. Phys.* **2009**, *11*, 4996–5009.

[48] Vasil'eva, I. A.; Voitova, N. A.; Nurmukhametov, R. N. Effect of the fluorine substitution in ethyl groups of 1,4-distyrylbenzene on the fine structure fluorescence and fluorescence excitation spectra *Optics and Spectroscopy* **2012**, *112*, 443–452.

[49] Gierschner, J.; Ehni, M.; Egelhaaf, H.-J.; Milián Medina, B.; Beljonne, D.; Benmansour, H.; Bazan, G. C. Solid-state optical properties of linear polyconjugated molecules: π-stack contra herringbone *The Journal of Chemical Physics* **2005**, *123*, 144914.

[50] Wykes, M.; Parambil, R.; Beljonne, D.; Gierschner, J. Vibronic coupling in molecular crystals: A Franck-Condon Herzberg-Teller model of H-aggregate fluorescence based on quantum chemical cluster calculations *The Journal of Chemical Physics* **2015**, *143*, 114116.

[51] Varghese, S.; Park, S. K.; Casado, S.; Fischer, R. C.; Resel, R.; Milián-Medina, B.; Wannemacher, R.; Park, S. Y.; Gierschner, J. Stimulated Emission Properties of Sterically Modified Distyrylbenzene-Based H-Aggregate Single Crystals *The Journal of Physical Chemistry Letters* **2013**, *4*, 1597–1602; PMID: 26282965.

[52] Spano, F. C. EXCITONS IN CONJUGATED OLIGOMER AGGREGATES, FILMS, AND CRYSTALS *Annual Review of Physical Chemistry* **2006**, *57*, 217–243; PMID: 16599810.

[53] Zhang, T.; Shi, W.; Wang, D.; Zhuo, S.; Peng, Q.; Shuai, Z. Pressure-induced emission enhancement in hexaphenylsilole: a computational study *J. Mater. Chem. C* **2019**, *7*, 1388–1398.

[54] Pawlak, R.; Vilhena, J. G.; D'Astolfo, P.; Liu, X.; Prampolini, G.; Meier, T.; Glatzel, T.; Lemkul, J. A.; Häner, R.; Decurtins, S.; Baratoff, A.; Pérez, R.; Liu, S.-X.; Meyer, E. Sequential Bending and Twisting around C–C Single Bonds by Mechanical Lifting of a Pre-Adsorbed Polymer *Nano Letters* **2020**, *20*, 652–657.

[55] Vilhena, J. G.; Pawlak, R.; D'Astolfo, P.; Liu, X.; Gnecco, E.; Kisiel, M.; Glatzel, T.; Pérez, R.; Häner, R.; Decurtins, S.; Baratoff, A.; Prampolini, G.; Liu, S.-X.; Meyer, E. Flexible Superlubricity Unveiled in Sidewinding Motion of Individual Polymeric Chains *Phys. Rev. Lett.* **2022**, *128*, 216102.

[56] Cacelli, I.; Prampolini, G. Parametrization and Validation of Intramolecular Force Fields Derived from DFT Calculations *J. Chem. Theory Comput.* **2007**, *3*, 1803–1817.

[57] Prampolini, G.; Livotto, P. R.; Cacelli, I. Accuracy of Quantum Mechanically Derived Force-Fields Parameterized from Dispersion-Corrected DFT Data: The Benzene Dimer as a Prototype for Aromatic Interactions. *J. Chem. Theory Comput.* **2015**, *11*, 5182–96.

[58] Cerezo, J.; Prampolini, G.; Cacelli, I. Developing accurate intramolecular force fields for conjugated systems through explicit coupling terms *Theor. Chem. Accounts* **2018**, *137*, 80.

[59] Prampolini, G.; da Silveira, L. G.; Vilhena, J. G.; Livotto, P. R. Predicting Spontaneous Orientational Self-Assembly: ¡i¿In Silico¡/i¿ Design of Materials with Quantum Mechanically Derived Force Fields *The Journal of Physical Chemistry Letters* **2022**, *13*, 243–250.

[60] Barone, V.; Cacelli, I.; De Mitri, N.; Licari, D.; Monti, S.; Prampolini, G. Joyce and Ulysses: Integrated and User-Friendly Tools for the Parameterization of Intramolecular Force Fields from Quantum Mechanical Data. *Phys. Chem. Chem. Phys.* **2013**, *15*, 3736–51.

[61] De Mitri, N.; Monti, S.; Prampolini, G.; Barone, V. Absorption and Emission Spectra of a Flexible Dye in Solution: A Computational Time-Dependent Approach *J. Chem. Theory Comput.* **2013**, *9*, 4507–4516.

[62] Prampolini, G.; Ingrosso, F.; Segalina, A.; Caramori, S.; Foggi, P.; Pastore, M. Dynamical and Environmental Effects on the Optical Properties of an Heteroleptic Ru(II)–Polypyridine Complex: A Multilevel Approach Combining Accurate Ground and Excited State QM-Derived Force Fields, MD and TD-DFT *J. Chem. Theory Comput.* **2019**, *15*, 529–545.

[63] Prampolini, G.; Ingrosso, F.; Cerezo, J.; Iagatti, A.; Foggi, P.; Pastore, M. Short- and Long-Range Solvation Effects on the Transient UV–Vis Absorption Spectra of a Ru(II)–Polypyridine Complex Disentangled by Nonequilibrium Molecular Dynamics *J. Phys. Chem. Lett.* **2019**, *10*, 2885–2891.

[64] Cerezo, J.; Garcia Iriepa, C.; Santoro, F.; Navizet, I.; Prampolini, G. Unraveling the contributions to the spectral shape of flexible dyes in solution: insights on the absorption spectrum of an oxyluciferin analogue. *Phys. Chem. Chem. Phys.* **2023**, *25*, 5007–5020.

[65] Frisch, M. J.; Trucks, G. W.; Schlegel, H. B.; Scuseria, G. E.; Robb, M. A.; Cheeseman, J. R.; Scalmani, G.; Barone, V.; Petersson, G. A.; Nakatsuji, H.; Li, X.; Caricato, M.; Marenich, A. V.; Bloino, J.; Janesko, B. G.; Gomperts, R.; Mennucci, B.; Hratchian, H. P.; Ortiz, J. V.; Izmaylov, A. F.; Sonnenberg, J. L.; Williams-Young, D.; Ding, F.;

Lipparini, F.; Egidi, F.; Goings, J.; Peng, B.; Petrone, A.; Henderson, T.; Ranasinghe, D.; Zakrzewski, V. G.; Gao, J.; Rega, N.; Zheng, G.; Liang, W.; Hada, M.; Ehara, M.; Toyota, K.; Fukuda, R.; Hasegawa, J.; Ishida, M.; Nakajima, T.; Honda, Y.; Kitao, O.; Nakai, H.; Vreven, T.; Throssell, K.; Montgomery, J. A., Jr.; Peralta, J. E.; Ogliaro, F.; Bearpark, M. J.; Heyd, J. J.; Brothers, E. N.; Kudin, K. N.; Staroverov, V. N.; Keith, T. A.; Kobayashi, R.; Normand, J.; Raghavachari, K.; Rendell, A. P.; Burant, J. C.; Iyengar, S. S.; Tomasi, J.; Cossi, M.; Millam, J. M.; Klene, M.; Adamo, C.; Cammi, R.; Ochterski, J. W.; Martin, R. L.; Morokuma, K.; Farkas, O.; Foresman, J. B.; Fox, D. J.; Gaussian˜16 Revision C.01; 2016; Gaussian Inc. Wallingford CT.

[66] TURBOMOLE V7.7 2022, a development of University of Karlsruhe and Forschungszentrum Karlsruhe GmbH, 1989-2007, TURBOMOLE GmbH, since 2007; available from `https://www.turbomole.org`.

[67] Smith, D. G. A.; Burns, L. A.; Simmonett, A. C.; Parrish, R. M.; Schieber, M. C.; Galvelis, R.; Kraus, P.; Kruse, H.; Di Remigio, R.; Alenaizan, A.; James, A. M.; Lehtola, S.; Misiewicz, J. P.; Scheurer, M.; Shaw, R. A.; Schriber, J. B.; Xie, Y.; Glick, Z. L.; Sirianni, D. A.; O'Brien, J. S.; Waldrop, J. M.; Kumar, A.; Hohenstein, E. G.; Pritchard, B. P.; Brooks, B. R.; Schaefer, H. F.; Sokolov, A. Y.; Patkowski, K.; DePrince, A. E.; Bozkaya, U.; King, R. A.; Evangelista, F. A.; Turney, J. M.; Crawford, T. D.; Sherrill, C. D. PSI4 1.4: Open-source software for high-throughput quantum chemistry *J. Chem. Phys.* **2020**, *152*, 184108.

[68] Cacelli, I.; Cerezo, J.; De Mitri, N.; Prampolini, G.; JOYCE2.10, a Fortran 77 code for intra-molecular force field parameterization. , available free of charge at http://www.iccom.cnr.it/en/joyce-2/, last consulted September 2022.

[69] Cerezo, J.; Santoro, F. FCclasses3: Vibrationally-resolved spectra simulated at the edge of the harmonic approximation *J. Comput. Chem.* **2023**, *44*, 626–643.

[70] Pronk, S.; Páll, S.; Schulz, R.; Larsson, P.; Bjelkmar, P.; Apostolov, R.; Shirts, M. R.; Smith, J. C.; Kasson, P. M.; van der Spoel, D.; Hess, B.; Lindahl, E. GROMACS 4.5: a

High-Throughput and Highly Parallel Open Source Molecular Simulation Toolkit *Bioinformatics* **2013**, *29*, 845–854.

[71] Berendsen, H. J. C.; Postma, J. P. M.; van Gunsteren, W. F.; DiNola, A.; Haak, J. R. Molecular dynamics with coupling to an external bath *J. Chem. Phys.* **1984**, *81*, 3684–3690.

[72] Bussi, G.; Donadio, D.; Parrinello, M. Canonical sampling through velocity rescaling *J. Chem. Phys.* **2007**, *126*, 014101.

[73] Parrinello, M.; Rahman, A. Polymorphic transitions in single crystals: A new molecular dynamics method *J. Appl. Phys.* **1981**, *52*, 7182–7190.

[74] Darden, T.; York, D.; Pedersen, L. Particle mesh Ewald: An N-log(N) method for Ewald sums in large systems *J. Chem. Phys.* **1993**, *98*, 10089–10092.

[75] Hess, B.; Bekker, H.; Berendsen, H. J. C.; Fraaije, J. G. E. M. LINCS: a linear constraint solver for molecular simulations *J. Comput. Chem.* **1997**, *18*, 1463–1472.

[76] Avila Ferrer, F. J.; Santoro, F. Comparison of vertical and adiabatic harmonic approaches for the calculation of the vibrational structure of electronic spectra *Phys. Chem. Chem. Phys.* **2012**, *14*, 13549–13563.

[77] Avila Ferrer, F. J.; Cerezo, J.; Stendardo, E.; Improta, R.; Santoro, F. Insights for an Accurate Comparison of Computational Data to Experimental Absorption and Emission Spectra: Beyond the Vertical Transition Approximation *J. Chem. Theory Comput.* **2013**, *9*, 2072–2082.

[78] Horng, M. L.; Gardecki, J. A.; Papazyan, A.; Maroncelli, M. Subpicosecond Measurements of Polar Solvation Dynamics: Coumarin 153 Revisited *J. Phys. Chem.* **1995**, *99*, 17311–17337.

[79] Karunakaran, V.; Senyushkina, T.; Saroja, G.; Liebscher, J.; Ernsting, N. P. 2-Amino-7-nitro-fluorenes in Neat and Mixed SolventsOptical Band Shapes and Solvatochromism *J. Phys. Chem. A* **2007**, *111*, 10944–10952; PMID: 17929778.

[80] Cardozo, T. M.; Aquino, A. J. A.; Barbatti, M.; Borges, I. J.; Lischka, H. Absorption and Fluorescence Spectra of Poly(p-phenylenevinylene) (PPV) Oligomers: An ab Initio Simulation *J. Phys. Chem. A* **2015**, *119*, 1787–1795.

[81] Oliveira, E. F.; Shi, J.; Lavarda, F. C.; Lüer, L.; Milián-Medina, B.; Gierschner, J. Excited state absorption spectra of dissolved and aggregated distyrylbenzene: A TD-DFT state and vibronic analysis *The Journal of Chemical Physics* **2017**, *147*, 034903.

[82] Milián-Medina, B. n.; Wasserberg, D.; Meskers, S. C. J.; Mena-Osteritz, E.; Bäuerle, P.; Gierschner, J. EDOT-Type Materials: Planar but Not Rigid *J. Phys. Chem. A* **2008**, *112*, 13282–13286.

[83] Stendardo, E.; Avila Ferrer, F.; Santoro, F.; Improta, R. Vibrationally Resolved Absorption and Emission Spectra of Dithiophene in the Gas Phase and in Solution by First-Principle Quantum Mechanical Calculations *Journal of Chemical Theory and Computation* **2012**, *8*, 4483–4493.

[84] Jorgensen, W. L.; Tirado-Rives, J. Potential Energy Functions for Atomic-Level Simulations of Water and Organic and Biomolecular Systems. *Proc. Natl. Acad. Sci. USA* **2005**, *102*, 6665–70.

[85] Ceriotti, M.; Fang, W.; Kusalik, P. G.; McKenzie, R. H.; Michaelides, A.; Morales, M. A.; Markland, T. E. Nuclear Quantum Effects in Water and Aqueous Systems: Experiment, Theory, and Current Challenges *Chem. Rev.* **2016**, *116*, 7529–7550; PMID: 27049513.